

Article

Preliminary Design Guidelines for Considering the Vibration and Noise of Low-Speed Axial Fans Due to Profile Vortex Shedding[†]

Gábor Daku *  and János Vad

Department of Fluid Mechanics, Faculty of Mechanical Engineering, Budapest University of Technology and Economics, Bertalan Lajos u. 4-6, H-1111 Budapest, Hungary; vad@ara.bme.hu

* Correspondence: daku@ara.bme.hu

† This paper is a revised version of our paper published in Proceedings of the European Turbomachinery Conference ETC14, Gdansk, Poland, 12–16 April 2021.

Abstract: This paper presents a critical overview on worst-case design scenarios for which low-speed axial flow fans may exhibit an increased risk of blade resonance due to profile vortex shedding. To set up a design example, a circular-arc-cambered plate of 8% relative curvature is investigated in twofold approaches of blade mechanics and aerodynamics. For these purposes, the frequency of the first bending mode of a plate of arbitrary circular camber is expressed by modeling the fan blade as a cantilever beam. Furthermore, an iterative blade design method is developed for checking the risky scenarios for which spanwise and spatially coherent shed vortices, stimulating pronounced vibration and noise, may occur. Coupling these two approaches, cases for vortex-induced blade resonance are set up. Opposing this basis, design guidelines are elaborated upon for avoiding such resonance. Based on the approach presented herein, guidelines are also developed for moderating the annoyance due to the vortex shedding noise.

Keywords: axial flow fan; blade vibration; low tip speed; preliminary fan design; vortex shedding



Citation: Daku, G.; Vad, J. Preliminary Design Guidelines for Considering the Vibration and Noise of Low-Speed Axial Fans Due to Profile Vortex Shedding. *Int. J. Turbomach. Propuls. Power* **2022**, *7*, 2. <https://doi.org/10.3390/ijtp7010002>

Received: 28 September 2021

Accepted: 4 January 2022

Published: 7 January 2022

Publisher's Note: MDPI stays neutral with regard to jurisdictional claims in published maps and institutional affiliations.



Copyright: © 2022 by the authors. Licensee MDPI, Basel, Switzerland. This article is an open access article distributed under the terms and conditions of the Creative Commons Attribution (CC BY-NC-ND) license (<https://creativecommons.org/licenses/by-nc-nd/4.0/>).

1. Introduction

Vortex shedding (VS) from low-speed axial flow fan rotor blades has become of engineering relevance in the past decades. The VS phenomenon discussed in this paper—termed herein as profile vortex shedding (PVS), and illustrated in Figure 1—is not to be confused with the trailing-edge-bluntness, VS, which takes place past the blunt trailing edge (TE) of the blade profile, acting as the aft portion of a bluff body [1]. In the aforementioned literature, PVS is referred to as a laminar-boundary-layer VS, because it can only occur if the boundary layer is initially laminar at least over one side of the blade profile. In this case, the initially laminar boundary layer, being separated near or after mid-chord position, reattaches in the vicinity of the TE—thus resulting in a separation bubble—and finally undergoes a laminar-to-turbulent transition. Moreover, the position and the size of the formed separation bubble plays a key role in tonal PVS noise emission. Recently, Yakhina et al. [2] published a detailed investigation about tonal TE noise radiated by low Reynolds number airfoils. They observed that a precondition for tonal noise emission is the formed separation bubble being sufficiently close to the TE. PVS may occur within a certain Reynolds number range. Based on the literature [3–5], a lower limit of $Re_c = 5 \times 10^4$ is assumed herein, while the upper limit is determined by the critical Reynolds number of the natural laminar-to-turbulent transition. When PVS is discussed for low-speed fans, as in the present paper, incompressible flow is considered by implying a Mach number of ≤ 0.3 .

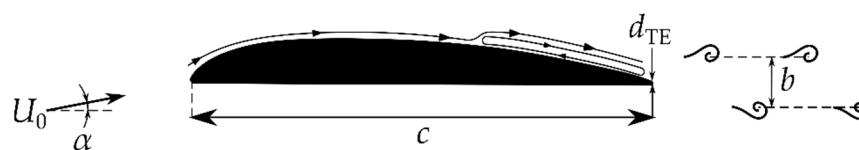


Figure 1. Profile vortex shedding (PVS).

Various models are available in the literature on the PVS phenomenon. In this paper, only the classic model by Tam [6] and Wright [7] is referred to, in order to provide a straightforward and comprehensive interpretation on the mechanism. According to this model, PVS is related to a self-excited feedback loop. Due to the unstable laminar boundary layer, Tollmien–Schlichting instability waves are generated; these waves travel downstream toward the TE where sound scattering occurs, and acoustic waves are created. The acoustic waves propagate upstream to amplify the original instabilities. If appropriate phase conditions are fulfilled, the disturbances are amplified at some frequencies, thus closing the feedback loop. Later, a number of authors, e.g., Nash et al. [8], carried out a critical revision on the aforementioned feedback loop model. PVS may generate vibration on the blade. As the studies by Ausoni et al. [9] suggest, the mechanisms of periodic vortex shedding and periodic blade vibration may mutually be coupled at a blade eigenfrequency, within a “lock-in” phenomenon.

In the case of low-speed axial flow fan blades, the difference between PVS and TE-bluntness VS in their physical mechanisms manifests itself in scaling techniques and the values of the Strouhal number being also different.

For blade profiles with thick or blunt trailing edges, the TE-bluntness vortex shedding [10] can be characterized by the Strouhal number based on the free-stream velocity U_0 and the TE thickness d_{TE} :

$$St_{TE} = f_{TE} d_{TE} / U_0 \cong 0.20 \quad (1)$$

For PVS [11,12], which is associated with the boundary layer transition and feedback mechanism:

$$St^* = f_{PVS} b / U_0 \cong 0.18 \quad (2)$$

where f is the dominant frequency of the two types of VS, and b is the distance between the vortex rows. Yarusevych et al. [11] found that St^* is universally valid for symmetrical, relatively thick NACA airfoils for certain ranges of the Reynolds number and angle of attack, suggesting the appellation of a “universal” Strouhal number St^* , as specified in Equation (2). However, these airfoils are not widely used in axial fan application; therefore, the present authors have extended the proposed St^* definition as follows. Systematic wind-tunnel experiments were performed on blade section models typical for low-speed axial fans, using a single-component hot-wire probe. Based on the measured f and b values, the authors also confirmed the validity of St^* for asymmetrical profile geometries, such as 8% cambered plate and RAF-6E profiles, in a quasi-2D experimental analysis [13]. Thus, the available experimental database on PVS frequency [5] was extended.

From an engineering point of view, the practical aspects of PVS are remarkable in two ways: vibration and noise. On the one hand, PVS creates a periodically fluctuating force normal to the chord, increasing the risk of blade vibration. On the other hand, VS appears as the primary source of the aeroacoustics noise of low-speed axial flow fans [14–16]. Hence, it is an important engineering objective to check and possibly to control the vibration and noise of low-speed axial fans due to the PVS that is already in the preliminary design phase. It is worth noting that the signatures of blade vibration and PVS-related noise may coincide in the frequency spectra. In [17], the vibrometer connected to the airfoil indicated a vortex-induced vibration, the dominant frequency of which coincided with that of the far-field tone.

Measurements on PVS in the literature are mostly related to isolated and steady airfoils [2,11–13,17,18]. Only a few studies dealt with PVS in the case of rotating blades of asymmetrical profiles being characteristic for realistic axial fans. Longhouse [19] detected

PVS noise on an axial fan of four cambered plate blades with a constant blade chord. Nevertheless, except for a small segment (~10%) of the span of one blade in near-tip region, the PVS noise was suppressed by aft-chord serrations. Furthermore, the spanwise variation of free-stream velocity tended to broaden the noise signature of PVS, thus acting against a remarkable, well-detectable tonal PVS character. Grosche and Stiewitt [20] examined a four-bladed propeller-type axial fan rotor with a moderate sweep and twist. They observed PVS noise at $\alpha \approx 4^\circ$ angle of attack, viewed in the rotating frame of reference near the blade tip, for three different Reynolds numbers based on the chord length ($Re_c = 9 \times 10^4, 1.3 \times 10^5, 2.6 \times 10^5$). All of the aforementioned observations—both the isolated blade profile and rotor consideration—suggest that the following blade features tend to increase the inclination for the occurrence of well-detectable tonal PVS: high aspect ratio (AR), low solidity, moderate twist, and constant blade chord. These parameters are typical for propeller-type fans [21]. Such propeller-type fans, where low-solidity is characteristic over a significant portion of the span, have been designed, for instance, by [22,23].

In order to moderate the harmful noise and vibration effects due to PVS, pessimistic design scenarios have systematically been discovered for which such harmful effects are pronounced. Furthermore, these design characteristics were coupled with rotor dynamics consideration. Based on this coupling, an exemplary unfavorable design case was set up in terms of both operational and geometrical characteristics, for which PVS demonstrates an increased risk of blade resonance. Taking the rotor of such an unfavorable design case—termed hereafter the PVS-affected rotor—as reference, approximate semi-empirical design guidelines can already be elaborated in the preliminary design phase for checking and possibly avoiding PVS-induced resonance. The design guidelines for noise reduction, reported in [13], have also been further developed toward a more detailed model, as illustrated in this paper.

2. Blade Vibration: An Overview

Turbomachinery blade profiles are suggested to be modeled in preliminary analysis as simple cantilever beams [24–30], which means that all degrees of freedom of the blades at the blade root, i.e., where connected to the hub, are constrained. The pure bending—or, in other words, transversal or flexural—vibrations of a prismatic beam with uniform cross-section according to time (τ) and the coordinate along the longitudinal direction of the beam (z) are described by the partial differential equation below, which is derived from the Euler-Bernoulli's beam theory [26,31]:

$$EI \frac{\partial^4 g(z, \tau)}{\partial x^4} + \rho_b A \frac{\partial^2 g(z, \tau)}{\partial \tau^2} = 0 \quad (3)$$

where $g(z, \tau)$ is the lateral displacement along the axis perpendicular to the blade chord; E is the Young modulus; I is the second moment of area with respect to the axis being parallel to the chord and fitting to the center of gravity (CG) of the blade section; A is the cross-sectional area of the blade profile; and ρ_b is the density of the blade material. The method of variable separation can be used to produce the free vibration solution. By utilizing the proper initial and boundary conditions, the i -th eigenfrequency (see later) and normal mode shape [31] can be expressed as follows:

$$F_i(z) = (\cos \beta_i z - \cosh \beta_i z) - \frac{(\cos \beta_i l + \cosh \beta_i l)}{(\sin \beta_i l - \sinh \beta_i l)} (\sin \beta_i z - \sinh \beta_i z) \quad (4)$$

where i is the order-number, i.e., 1, 2, 3 etc.; $F(z)$ is the characteristic function or the normal mode of the beam; l is the radial extension of blade from hub to tip, i.e., the blade span, and $\beta_i l \approx (2i - 1)\pi/2$. For illustrative examples, Figure 2 qualitatively presents the shapes for some bending modes, generated on the basis of Equation (4). The vertical axis represents the normal mode (i.e., dimensionless displacement) and the horizontal axis shows the dimensionless length of the beam.

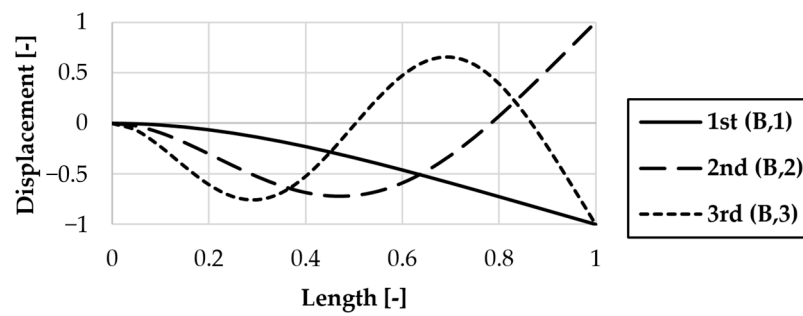


Figure 2. Normal bending modes of the beam.

The pure torsion of the cantilever beam is governed by the following differential Equation [32]:

$$GI_t \frac{\partial^2 \zeta(z, \tau)}{\partial x^2} + \rho_b I_p \frac{\partial^2 \zeta(z, \tau)}{\partial \tau^2} = 0 \quad (5)$$

where $\zeta(z, \tau)$ is the rotation angle around the longitudinal direction of the beam; G is the shear modulus; I_t is the torsional stiffness or torsional constant; and I_p is the polar moment of area of the blade section.

It is important to note that in practice, mixing of modes can occur, and accordingly, various researchers have executed studies on experimental and theoretical evaluations of flexural-torsional vibration analysis, taking into account the coupling of flexural and torsional modes, e.g., [24,27,28,31,33,34]. The present authors have only dealt with pure bending and torsional vibration modes, keeping in mind the simplest possible analytical description mode.

In the literature, basic concepts are available for the analytical treatment of the vibration of beams/blades affected by centrifugal force field due to their rotation. Such concepts regard both untwisted [31] and twisted [24,28,29] geometries. As discussed in [25], the centrifugal force originating from the rotation of the blades has a stiffness-increasing effect, i.e., it tends to moderate the inclination of the blade to vibrate. At the present state of research, the authors neglect the mechanical effect of the centrifugal field, for the following reasons: (a) The centrifugal field tends to be of moderate significance in the low-speed fan blades discussed herein; and (b) the intention is to make a pessimistic—i.e., safety-increasing—preliminary design approach via neglecting the stiffness-increasing trend due to the centrifugal field. Blade twist tends to reduce the bending eigenfrequencies, as FEM computations (not presented herein) demonstrate. Therefore, for twisted blades, the critical frequencies of excitation tend to be shifted toward lower values. At the present state of research, the authors neglect the mechanical effect of blade twist. The reasonability of such neglect is commented on later on. The concerted review of the effects of centrifugal force field and blade twisting, or taking into account the mixing of the pure vibration modes, is planned to be the subject of future research.

Even mechanical or fluid mechanical excitations can unavoidably induce the vibration of the axial flow fan blade to a certain extent, as well as being a source of vibration in the structure on which it is installed. Such excitation effect may derive from the interaction of the fan blades with the wake developing behind the elements placed upstream of the rotor e.g., supporting struts, inlet guide vanes, or even from the discussed PVS phenomenon. For instance, corresponding to the pressure rise, a steady mean lift force acts on the blade. However, the lift force also has a varying component e.g., the fluctuating force due to PVS. As detailed by [25,35], both forces produce a bending moment, resulting in vibration. If the dominant frequency of PVS coincides with an eigenfrequency of the blade, resonance may occur, and the intensity of the vibration can only be limited if the mechanical structure is stiff enough or damped sufficiently. Therefore, it is to be treated with special care in the case of fan blades made of cambered sheet metal plates because their eigenfrequency—due to the moderate inertia of the cross-section and the resulting lower stiffness—is lower compared to that of the profiled blades [25].

Even though fans commonly operate with mechanical stresses far below the capacity of their material—and thus the vibration of the fan blade due to resonance does not lead to the fracture of the mechanical structure—, in the presence of the corresponding stresses, which reach a maximum near the blade root, there can be a risk of fatigue fracture. These stresses combine with the centrifugal ones; therefore, a mixed type, alternating stress condition appears, which must be considered in the design of the fan.

Furthermore, the rotor may become imbalanced due to the deformation patterns associated with each resonance frequency of the blade, forcing the shaft to bend, escalating the initial imbalance and bending. If the excitation is sufficiently intense, resulting in a vibration of large amplitude, one of the fan blades can rub into the duct walls leading to rotor imbalance or the breaking down of the blades.

2.1. Analytical Treatment

2.1.1. Bending Modes

In order to provide a straightforward and comprehensive approach in preliminary design, avoiding any need for numerical computation at the present phase of research and as a solutions of Equation (3), the following analytically expressed eigenfrequencies are considered for the bending modes of an arbitrary prismatic rod, as specified in the literature [26]:

$$f_{B,i} = \frac{K_{B,i}}{l^2} \sqrt{\frac{E I}{A \rho_b}} \quad (6)$$

Namely, the simple analytical formula above can easily be extended to higher-order bending modes by substituting the appropriate $K_{B,i}$ constant into Equation (6). The values of $K_{B,i}$ for the first three bending modes are $K_{B,1} = 0.560$, $K_{B,2} = 3.506$ and $K_{B,3} = 9.819$, respectively.

2.1.2. Torsional Modes

By solving the expression in Equation (5), the eigenfrequency for torsional modes can be obtained using the analytical formula e.g., in [26], as follows:

$$f_{T,i} = \frac{i - 0.5}{2l} \sqrt{\frac{G I_t}{\rho_b I_p}} \quad (7)$$

In Equation (7) every variable can be determined—except I_t —by utilizing the material and geometrical parameters of the blade. To calculate the I_t torsional constant for a flat plate, the following relation is given in [26]:

$$I_t = K_t c t^3 \quad (8)$$

where c is the chord length (width of the plate); t is the thickness (height of the plate); and K_t is a mechanical constant which can be obtained from Figure 4.2 of [26] or calculated applying the formula—being in accordance with the former literature—e.g., [36]. However, the aforementioned alternatives for determining the torsion constant are related not to a cambered but to a flat plate, inhibiting their direct application in our case study. To overcome this problem, based on [36–38], the torsional constant of a thin-walled open tube cross-section of uniform thickness can be expressed as:

$$I_t = \frac{1}{3} U t^3 \quad (9)$$

where U is the length of the midwall perimeter, shown dashed later in Figure 5.

2.2. Finite Element Method (FEM)

The FEM is a useful and generally accepted tool for solving engineering problems numerically, such as the modal analysis of rotor blades [39–41]. The desired mechanical characteristics can be computed by dividing an arbitrary mechanical structure into simple geometric shapes and defining the material properties and governing connections among these elements. In this study, the frequency analysis of a low speed axial fan blade is carried out using a commercial FEM software program ANSYS Mechanical APDL 2019 R3.

2.2.1. Geometry, Materials, and Elements

In the present paper, the hub is assumed to be rigid in comparison to the fan blade, thus all degrees of freedom of the blades at the hub, i.e., at the blade root, are constrained. Therefore, only one segment of the axial flow fan composed of a single blade without a hub part was examined. In accordance with the later investigated PVS-affected rotor blade profile of the circular-arc-cambered plate of 8% relative curvature and the dimensional and dimensionless values of Tables 3 and 5, the necessary geometrical characteristics for 3D modeling are summarized in Table 1. The reason for choosing this blade profile geometry will be explained in detail later in Section 3.2. For the FEM case study, the fan blade is made of structural steel with a density of 7850 kg/m³, a Young's modulus of 200 GPa, and a Poisson's ratio (ν_P) of 0.3.

Table 1. Blade geometrical and material parameters for the FEM case study.

l	c	t	h	ρ_b	E	ν_P
264 mm	120 mm	2.40 mm	9.60 mm	7850 kg/m ³	200 GPa	0.30

According to the literature [30,39], SHELL 181 element is suitable for analyzing thin to moderately-thick shell structures related to turbomachinery blades, such as wind turbine and axial flow fan blades. Hence, this type of element is applied to model the fan blade with 124 nodes in the axial direction and 256 nodes in the radial direction. Basically, SHELL 181 is a four-node element with six degrees of freedom at each node: translations in the x , y , and z directions and rotations about the x , y , and z -axes. However, it should be mentioned that the same solution could be obtained by using the 20-node Hex20 (SOLID 186) element of Ansys Workbench 2019 R3.

2.2.2. Mesh Convergence

A mesh convergence study was performed to assure the optimum mesh number in terms of computational accuracy. The first three bending (B) and torsional (T) eigenfrequencies of the fan blade are computed in several mesh sizes (the element number varies from 258 to 507,904). By increasing the number of elements, the first bending eigenfrequency increases slightly and then becomes nearly constant. For higher-order bending and the torsional mode, similar effects can be observed. As shown in Figure 3, 31,744 elements are appropriate to get a sufficiently accurate solution. Nevertheless, it should be mentioned that even a model with a lower number of elements is sufficient for the third-octave band prediction of the first bending eigenfrequency (see Appendix A).

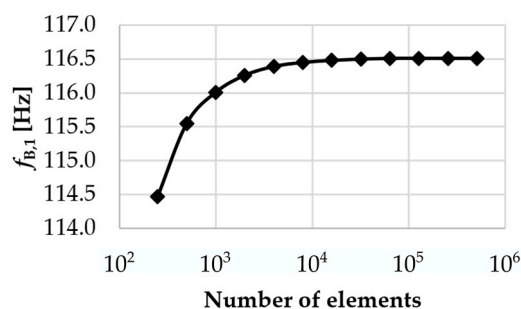


Figure 3. Mesh convergence study.

2.3. Comparison of the Results

In Table 2, the first three analytical bending (B) and torsion (T) eigenfrequencies were calculated based on Equations (5), (7) and (8), and compared to the eigenfrequency obtained by means of FEM. The first column indicates the vibration mode case under discussion. In the second and the fourth columns, FEM and the analytical eigenfrequencies are summarized, respectively. In the third and the fifth columns, the appropriate band number of the third-octave band resolution is listed in accordance with Appendix A. The “Discrepancy” column contains the relative discrepancy of $f_{\text{analytical}}$ in comparison to f_{FEM} .

Table 2. Geometrical and material parameters of the blade.

Mode	f_{FEM} [Hz]	1/3 Octave Band No.	$f_{\text{analytical}}$ [Hz]	1/3 Octave Band No.	Discrepancy [%]
B,1	116.5	11	116.1	11	0.3
B,2	595.2	18	727.6	19	18.2
B,3	1146.7	21	2037.8	23	43.7
T,1	140.1	11	117.4	11	19.4
T,2	472.8	17	352.1	15	34.3
T,3	949.6	20	586.9	18	61.8

From Table 2, it can be observed that the analytical treatment for the first bending (B,1) eigenfrequency is in good agreement with the FEM result. Nevertheless, for the higher-order bending and the torsional modes, the relative discrepancy between analytical and FEM results becomes greater and tends to increase with the increasing of the order of the modes. A possible explanation for this is the partial violation of the briefly presented Euler–Bernoulli thin beam theory. Hence, the AR of the beam is equal to 2.2; namely, the beam is not considered to be slender ($AR > 10$).

Although there have been alternative methodologies to obtain a more accurate analytical prediction for short beams ($AR < 10$), e.g., Timoshenko’s beam theory [31], the present paper focuses on Euler–Bernoulli’s beam theory, due to the following reasons. (a) On the one hand, the authors aim to create a closed analytical formula with the most straightforward possible analytical description in mind. (b) On the other hand, as shown in [31,42], the relative discrepancy between the analytical first bending eigenfrequencies, calculated based on the two different theories, is less than 5–10%, which, fitting for point (a), is considered to be an acceptable approximation. Based on this and the highlighted role of the first bending mode detailed in Section 3.1, the confirmation of the analytical model by FEM is of primary significance for the first bending mode only and is of secondary importance for the other modes.

Despite the simplification assumption discussed at the beginning of the chapter (untwisted and non-rotating fan blade), supplementary FEM case studies were carried out for the twisted and rotating blade as well. The FEM results demonstrated that both the blade twisting and the presence of a centrifugal force field have a bending eigenfrequency-reducing effect, providing an upper estimation for the first bending eigenfrequency of the blade. As the later calculation example illustrates, even in the case of the untwisted and

stationary fan blade, only impractically low tip speeds would result in the coincidence of the first bending eigenfrequency and PVS frequency. Therefore, the simplified fan blade model applied by the present authors can be considered as a pessimistic design scenario.

3. Blade Mechanics: An Exemplary Case Study

3.1. The Importance of the First-Order Bending Mode

The risk in fan operation due to blade vibration is simultaneously viewed in the present paper from the following two perspectives, which are related to each other. (a) The risk of instantaneous reduction of the gap between the blade tip and the casing. From the perspective of the tip gap reduction, the vibration modes exhibiting monotonously increasing deformation amplitude along the blade height are considered the riskiest. These are the first bending and first torsional modes. (b) The risk of instantaneous rotor imbalance. This occurs in cases when the weight point of the entire blade is displaced in the transversal direction from its original position, fitting on the (approximately) radial blade stacking line, for which the rotor has originally been balanced. From the perspective of rotor imbalance, none of the torsional modes are considered to be risky, as they tend to leave the weight point of the entire blade (approximately) in its original position. In addition, according to their wavy vibration pattern, higher-order bending modes are considered to exhibit only a moderate transversal displacement of the blade weight point.

Therefore, among the various vibrational modes caused by PVS excitation, the first bending mode is judged to be the most critical, and the higher-order bending modes and torsional modes are considered of secondary significance. Consequently, out of the analytical solutions in Equation (5), the “first-order bending mode” is taken herein as an illustrative example of the analytical treatment elaborated upon by the authors. Nevertheless, the reasonability of this choice is justified and supported by the subsequent examples, as follows.

The impact of PVS on both noise and vibration is presumed by the present authors to be pronounced when extensive and coherent vortices are shed with uniform frequency along a dominant portion of the blade span. In this case, PVS is assumed to exhibit pressure fluctuations over the blade suction and pressure surfaces, causing chord-normal forces. Assuming spanwise and spatially coherent shed vortices, the resultant fluctuating forces are in phase over the entire span. Furthermore, PVS and the associated forces may occur farther upstream of the TE (cf. [12]). Such a PVS-induced excitation likely triggers the first-order bending mode.

An upstream stator, e.g., the nearly radially aligned supporting struts located upstream of the rotor, is able to cause wake-blade—also known as “rotor-stator”—interaction, in which the upstream wakes of the stator are swept downstream into the axial flow fan blade-row. The wakes are parallel with the relative velocity (w), thus the interaction manifests itself as a nearly simultaneous, spatially coherent aerodynamic excitation along the entire blade span. Hence, the fan blades are acted by chord-normal fluctuating force, resulting in a spatially coherent bending moment rather than torsional.

In addition, in [25] as a general approach, the frequency of the first bending mode of the blades is to be kept far away from the frequencies of excitation. As it was just mentioned, elements located upstream of the rotor—supporting struts and inlet guide vanes—cause rotor–stator interaction as aerodynamic excitation to the rotor blades, occurring at a frequency of rotational frequency multiplied by the number of upstream elements. On the other hand, such excitation effects correspond to rotor imbalance (“shaker effect”) appearing as mechanical excitation at the rotational frequency of the fan.

Moreover, as illustrated in [5], the fluctuation of chord-normal force due to PVS may lead to a variance of the lift coefficient in the order of a magnitude of ± 10 percent of the temporal mean value. As demonstrated in [35], the varying component of lift force causes a bending moment on the blade. When extensive and coherent vortices are shed with uniform frequency along a dominant portion of the blade span, they represent spatially coherent elemental aerodynamic excitation forces, being in phase over the elemental blade

sections, and thus, integrated into a pronounced overall bending moment. The phase identity of the elemental excitation forces along the blade span matches with the phase identity of blade deformation in the first bending mode of the blade, if the frequency of PVS matches with the eigenfrequency related to the first bending mode.

3.2. Eigenfrequency

In order to build up a straightforward model for the interaction of the blade and the fluctuating aerodynamic force due to PVS, some simplifications must be introduced. First of all, a circular-arc-cambered plate of 8% relative curvature is chosen as a blade profile for several reasons:

- At moderate Reynolds numbers and angles of attack (α), the cambered plate produces reasonably high C_L , that is comparable with an airfoil profile, i.e., RAF-6E [43], thus enabling the design of blades of relatively high specific performance, i.e., utilizing the loading capability of the blade sections.
- At 8% relative curvature, the lift-to-drag (LDR) is near the maximum among the cambered plates of various relative camber, thus enabling the design for reasonably high efficiency [44].
- In accordance with the aforementioned practical aspects, it is a cambered plate of 8% relative camber for which hot-wire measurement data are made available by the present authors on PVS at different free-stream velocities and angles of attack [13]. As per the illustration, Figure 4 shows C_L , C_D , and LDR values as a function of the angle of attack for the 8% cambered plate.

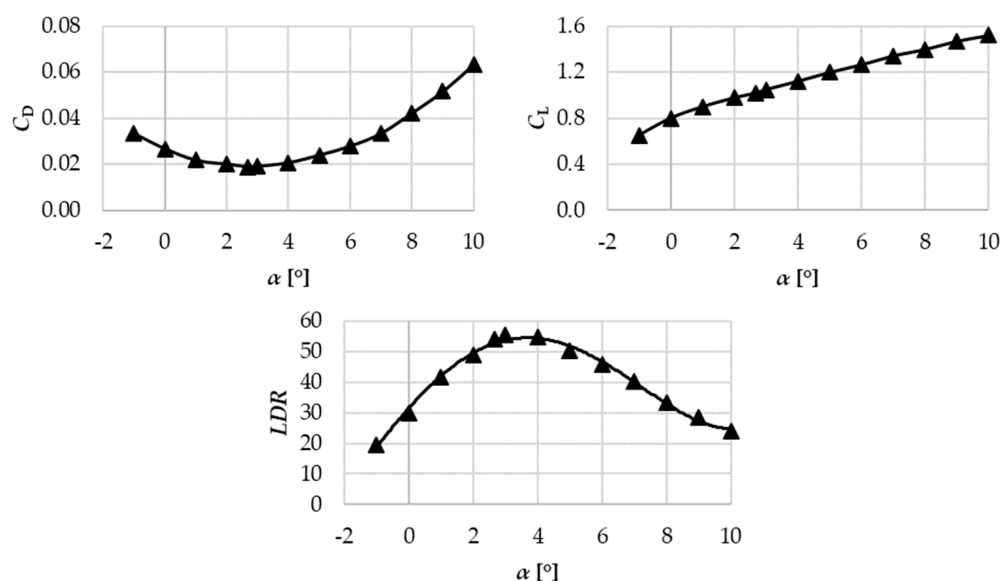


Figure 4. Lift and drag coefficients and lift-to-drag ratios as a function of angle of attack for 8% cambered plate at $Re_c = 3 \times 10^5$ measured by Wallis [44].

Secondly, the fan blade is presumed to consist of geometrically identical blade sections along the full span. This means that the blade chord c , plate thickness t , and height of the camber line h are constants (Figure 5). The measurement data presented by [44] and shown in Figure 4, are related to a relative thickness (t/c) of 2%. This value is representative in fan manufacturing; therefore, t/c is fixed at 2% for the present investigations.

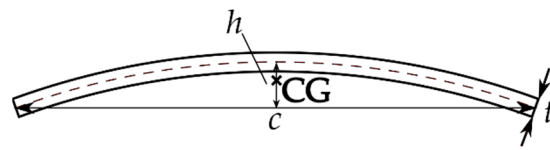


Figure 5. Circular-arc-cambered plate (8% relative camber).

Finally, as discussed earlier, it is assumed that all degrees of freedom of the blades at the hub, i.e., at the blade root, are constrained. This is a reasonable approximation; e.g., if sheet metal blades connect to the hub with a welded joint, or, in the case of polymer material, if the entirety of the hub and blading assembly is injection-molded as a single product. The simplifications above enable us to model the blade as a cantilever beam (or clamped beam) subjected to free vibration. In accordance with Section 3.1, the lowest eigenfrequency, related to the first-order bending mode, can be calculated as follows:

$$f_{B,1} = \frac{0.56}{l^2} \sqrt{\frac{I}{A}} \sqrt{\frac{E}{\rho_b}} \tag{10}$$

The last term on the right-hand side of Equation (10), as the square root of the specific modulus E/ρ_b , is termed herein the wave propagation speed, and denoted as a_b . This is actually the acoustic wave propagation speed in a long one-dimensional fictitious beam made of the blade material. The resultant swinging pattern is shown in Figure 6.

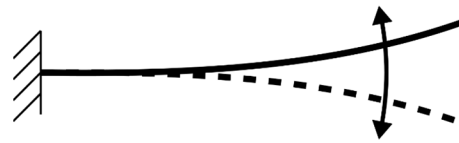


Figure 6. Cantilever beam subjected to free vibration (perpendicular to the blade chord).

3.3. Second Moment of Area

The purpose of the present section is to demonstrate how the I/A term can be related to the basic geometrical characteristics of the circular-arc-cambered plate blade (c , h/c , t/c), creating a direct relationship between the first eigenfrequency and the geometrical parameters of the blade. However, no closed analytical relationship exists in the literature for such purpose. Therefore, an alternative method must be found to express the second term of the right-hand side of Equation (10) with the use of blade geometrical parameters, such as c , h , and t . As a first step, the second moment of area of a cambered plate and a flat plate with same geometrical parameter (t , c) were compared to each other.

The quotient of the second moment of area and the cross-section, in case of a flat plate is:

$$(I/A)_{\text{flat}} = (ct^3/12)/(ct) = t^2/12 \tag{11}$$

For a cambered plate it is:

$$(I/A)_{\text{cambered}} = K_1(I/A)_{\text{flat}}, \text{ where } K_1 = K_1(t/c, h/c) \tag{12}$$

I_{cambered} was obtained for the cambered plate-section using an analytical integration process known from basic solid-state mechanics [45]. As background information for the reader, the values of K_1 are presented in Figure 7 for representative relative thickness and relative camber (h/c) values. For the fitted curves in Figure 7, K_1 was calculated for fixed t/c values for uniform steps of 0.01 h/c over the entire h/c range. In the blade design presented later, K_1 ($t/c = 0.02$; $h/c = 0.08$) = 18.07 was used, in accordance with the previously selected blade geometrical parameters.

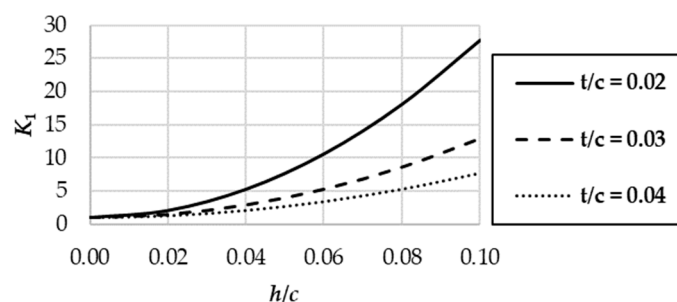


Figure 7. The value of K_1 as a function of relative camber for various relative thicknesses.

Substituting Equations (11) and (12) into Equation (10), the first bending eigenfrequency can be expressed as follows:

$$f_{B,1} = \frac{0.56}{l^2} \sqrt{K_1 \frac{t^2}{12}} a_b = \frac{0.56}{l^2} K_b t a_b \quad (13)$$

where $K_b = K_b (t/c = 0.02; h/c = 0.08) = 1.23$ is the blade mechanics coefficient. Case studies considering other t/c and h/c values can be carried out using Figure 7.

4. PVS-Affected Rotor: An Exemplary Case Study

The aim of this section is to outline a design case study, resulting in a rotor suspected to be unfavorable in terms of noise and vibration due to PVS. Although several unfavorable design cases of such kind can be intentionally generated, this paper intends to present a single, representative design example. The resultant rotor will be termed herein the PVS-affected rotor. Such a design aims to serve as a basis for the realization of a case study rotor that is expected to exhibit remarkable and experimentally well-detectable narrowband signatures of PVS. By such means, the orders of the magnitude of harmfulness of PVS-related effects are to be quantified in future experiments on the PVS-affected rotor, in comparison with other rotors of comparative design. The features of the PVS-affected rotor are as follows:

- (a) The rotor blading tends to exhibit a PVS of spanwise constant frequency, and thus, is theoretically presumed to realize large-scale, spatially coherent vortices over the dominant portion of the blade span. Such coherent vortices are assumed to cause spatially correlated, narrowband noise, as well as mechanical excitation over the dominant part of span at a given frequency. The condition of spanwise constant PVS frequency is therefore applied herein in a pessimistic aspect, although it is noted that the signature of PVS noise was observed by [19] even when PVS was confined to ~10% span near the tip of a single blade.
- (b) The latter is presumed to provoke blade vibration, if the frequency of PVS coincides with the frequency of the first bending mode of blade vibration.

4.1. Aerodynamics: Blade Design

To be able to design a fan for which the spanwise constancy of PVS frequency is fulfilled—thus satisfying Equation (14), presented later—first, typical dimensionless design and geometrical characteristics, representative of propeller-type fans, were systematically gathered and summarized in Table 3. Here, the authors stress that, in order to guarantee the validity of Equation (9), the blade chord along the blade span was fixed, so $c(r_b) = \text{constant}$. The tendency toward keeping the chord constant along the span in the blade design is supported by the literature examples of [19,20]. Based on the well-known Cordier diagram [46] for turbomachines of favorable efficiency, axial flow fans have the specific diameter and the specific speed within the approximate ranges of $1 \leq \delta \leq 1.5$ and $2 \leq \sigma \leq 3$, respectively. These ranges correspond to the global total pressure rise coefficient and flow coefficient within the ranges of $0.05 \leq \Psi_t \leq 0.25$ and $0.1 \leq \Phi \leq 0.5$, respectively. Thus, values in Table 3 fit to the Cordier diagram well. Regulation 327/2011/EU5 issued energy

efficiency requirements regarding fans in the EU [47], driven by motors with an electric input power between 125 W and 500 kW. According to this, the target total efficiency of an axial fan is $0.5 \leq \eta_t \leq 0.6$ depending on the arrangement and input power. Considering a more economical operation, we are moving toward higher efficiency levels; therefore, $\eta_t \approx 0.7$ is chosen.

Table 3. Geometrical and material parameters of the blade for the PVS-affected rotor.

c/D_{tip}	ν	AR	Ψ_t	Φ	N	η_t	δ	σ
0.133	0.415	2.22	0.143	0.309	5	0.700	1.11	2.39

The first two parameters as well as N in Table 3 define the blade solidity from hub to tip. When calculating the solidity (c/s), it is found that it is below 0.7 along the entire radius of the blade even at the hub, as can be observed in Figure 8. Therefore, according to [46] measurement data on isolated blade profiles—such as data included in Figure 4 in the case of a 8% cambered plate—can be applied in the present design of the PVS-affected rotor. In addition to the aerodynamic data in Figure 4, the empirical data on PVS in [5,13] are also related to isolated profiles, thus fitting to the low-solidity approach utilized herein.

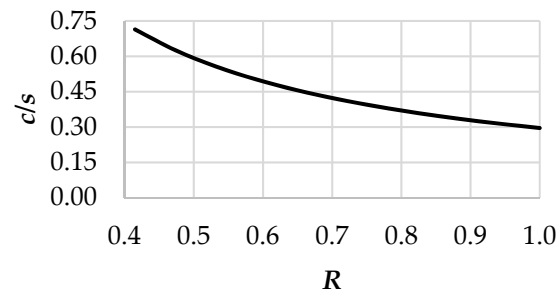


Figure 8. Blade solidity as a function of dimensionless radius ($R = r/r_{\text{tip}}$).

In what follows, preliminary design efforts are made for obtaining a rotor blading exhibiting PVS of spanwise constant frequency in order to fulfill the pessimistic condition outlined at the end of the Introduction. The PVS frequency can be expressed from Equation (2) as follows:

$$f_{\text{PVS}}(r_b) = St^* \frac{U_0(r_b)}{b(r_b)} = \text{const} \quad (14)$$

A nearly constant value of $St^* \approx 0.19$ was found for a 8% cambered plate for various Reynolds numbers and angles of attack in the present authors' previous measurement campaign [13]. Keeping the uncertainty of the measurement-based St^* data in mind, this value is in fair agreement with the literature-based data in Equation (2). $St^* = 0.19$ was used for the calculation presented in the paper. In order to clarify the trend of the free-stream velocity, the velocity vectors are shown in Figure 9. Based on Figure 9, the square of the free-stream velocity can be written as follows [46]:

$$U_0^2(r_b) = c_x^2(r_b) + \left(u(r_b) - \frac{\Delta c_u(r_b)}{2} \right)^2 \quad (15)$$

where c_x is the axial velocity component; u is the circumferential velocity; and Δc_u is the increase of tangential velocity due to the rotor.

the rotor is neglected; therefore, $W(R)$ is calculated from only the local flow coefficient $\varphi = c_x(r_b)/u_{\text{tip}}$ and the dimensionless radius corresponding to the rigid body rotation. In the present methodology, uniform axial inlet condition is assumed, $c_x(r_b)/u_{\text{tip}} = \text{constant}$. Furthermore, based on [46] as an approximation, the change of meridional—i.e., axial—velocity is neglected through the rotor. The above implies that spanwise constant axial velocity is presumed, as a brief approximation.

As a next step, based on the value of $W(R_{\text{mid}})/C_D(R_{\text{mid}})$, the drag coefficients are determined along the blade span. As described earlier, the $C_D(R)$, $\alpha(R)$ and $C_L(R)$ data are assigned to each other, via Figure 4. As a next stage of the design, $\Delta c_u/u_{\text{tip}}$ is expressed from the simplified work equation of an elemental rotor:

$$\frac{c}{s(r_b)} C_L(r_b) \cong \frac{2\Delta c_u(r_b)}{U_0(r_b)} \quad (20)$$

where $s = 2r_b\pi/N$ is the blade spacing. With the knowledge of $\Delta c_u(R)/u_{\text{tip}}$, the local isentropic total pressure rise coefficient $\psi_{t,\text{is}}(R)$ is expressed from the Euler equation of turbomachines:

$$\Delta p_{t,\text{is}}(r_b) = \rho_a u(r_b) \Delta c_u(r_b) \quad (21)$$

here $\Delta p_{t,\text{is}}$ is the isentropic total pressure rise, and ρ_a is the density of air. This computed $\psi_{t,\text{is}}(R)$ is then substituted into Equation (16) for calculating a new approximation of $W(R)$ in the next iteration loop. Fast convergence is obtained in two to three iteration loops. The results are judged to be converged if the relative difference in $\psi_{t,\text{is}}(R)$ for the consecutive iteration steps becomes less than 2%.

A feature of the iterative method is that $\psi_{t,\text{is}}(R)$ and $\alpha(R)$ are actually the results of the design process. The spanwise distributions of the calculated quantities are shown in Figure 10, where $\gamma(R)$ is stagger angle measured from the circumferential direction. Annulus-averaging of $\psi_{t,\text{is}}(R)$ represents the global isentropic total pressure rise obtained as Ψ_t/η_t , using the data in Table 3.

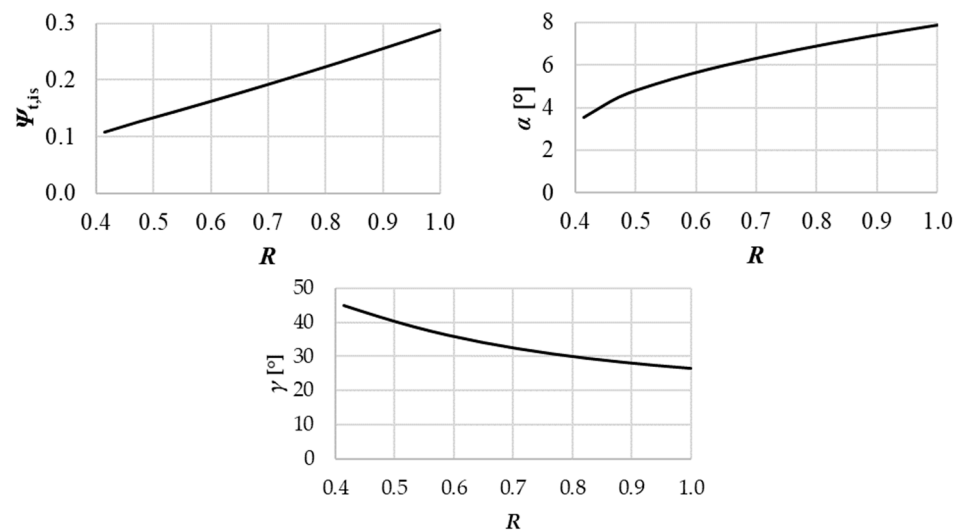


Figure 10. Calculated distributions $\psi_{t,\text{is}}(R)$, $\alpha(R)$, and $\gamma(R)$ as a function of R .

Figure 11 represents the proportionate three-dimensional model of the designed PVS-affected fan. The rotor has a realistic, common geometry, as it is representative of propeller-type axial flow industrial fans. The blade geometry is in accordance with the fact that, as a manufacturing simplification, low-speed axial fan blades of cost-effective manufacturing can be made from a plate of spanwise constant chord, as they are rolled in such a way that spanwise constant camber and moderate twist occur.

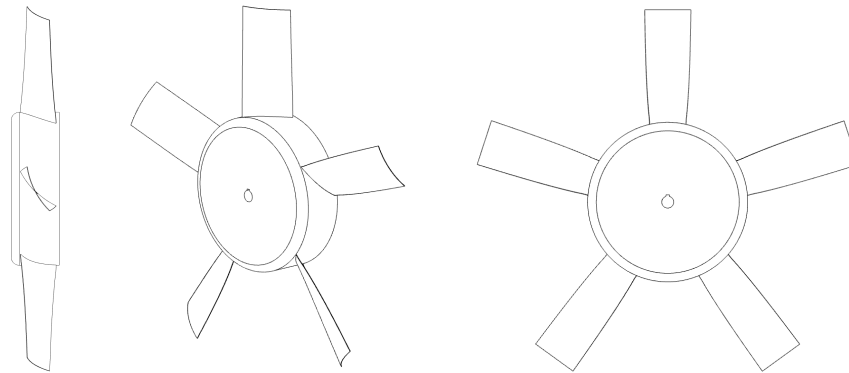


Figure 11. The PVS-affected fan rotor.

4.2. Mechanically or Acoustically Unfavorable Design Cases

In order to set up mechanically unfavorable design cases, representing a coincidence of the frequency of PVS with the frequency of the first bending mode of blade vibration, it is necessary to express U_0 and b in Equation (14). However, b was previously expressed, as shown in Equation (17). Therefore, it is only necessary to deal with U_0 . Based on Equations (20) and (21), the free-stream velocity is written as follows:

$$U_0(r_b) = \frac{2\Delta p_{t, is}(r_b) s(r_b)}{\rho_a u(r_b) c C_L(r_b)} \quad (22)$$

Thus, the PVS frequency can be expressed from Equations (14), (19) and (22):

$$f_{PVS}(r_b) = St^* \frac{2\Delta p_{t, is}(r_b) s(r_b)}{\rho_a c C_L(r_b) u(r_b)} \frac{2}{K^* C_D(r_b) c} \quad (23)$$

With the use of $s(r_b)/u(r_b) = (2 r_b \pi / N) / (2 r_b \pi n) = 1 / (nN)$ and $C_D = C_L / LDR$, Equation (23) is written as follows:

$$f_{PVS}(r_b) = St^* \frac{2\Delta p_{t, is}(r_b)}{\rho_a c C_L(r_b)} \frac{1}{N} \frac{2 LDR(r_b)}{n K^* C_L(r_b) c} \quad (24)$$

where N is the blade count and n is the rotor speed. The right-hand side of Equation (24) can be rearranged according to Equation (25) in the following way: In the first term, the global aerodynamic performance characteristics are grouped. The second term represents the operational condition of the rotor. In the third term, the basic parameters of the blade geometry are gathered. The fourth term represents the aerodynamics parameters of the elemental blade section. Finally, the last term incorporates the empirics and coefficients.

$$f_{PVS}(r_b) = \frac{\Delta p_{t, is}(r_b)}{\rho_a} \frac{1}{n} \frac{1}{N} \frac{LDR(r_b)}{c^2} \frac{4 St^*}{C_L^2(r_b) K^*} \quad (25)$$

In order to obtain generalized conclusions and trends, dimensionless quantities and groups must be introduced. It should be emphasized that PVS frequency is constant along the blade span due to the presented fan design method. Therefore, any characteristic taken at an arbitrary r_b radius can be replaced by the same characteristic taken at R_{mid} . Furthermore, as a brief approximation $\eta_t(r_b) = \eta_t(R_{mid}) \approx \text{constant}$ is presumed. With respect to the foregoing, the first term on the right-hand side of Equation (25) can be expressed:

$$\frac{\Delta p_{t, is}(r_b)}{\rho_a} = \frac{\Delta p_{t, is}(R_{mid})}{\rho_a} = \frac{\Delta p_t(R_{mid})}{\rho_a \eta_t(R_{mid})} = \frac{\Psi_t(R_{mid})}{\eta_t} \frac{u_{tip}^2}{2} \quad (26)$$

where $u_{\text{tip}} = D_{\text{tip}}\pi n$ is the tip circumferential speed. The second and the third terms are written as follows:

$$\frac{1}{n} \frac{1}{c^2 N} = \frac{1}{n} \frac{1}{D_{\text{tip}}\pi} D_{\text{tip}}\pi \frac{1}{c^2 N} = \frac{1}{u_{\text{tip}}} s_{\text{tip}} \frac{1}{c^2} \quad (27)$$

Thus Equation (25):

$$f_{\text{PVS}}(R_{\text{mid}}) = \frac{\Psi_t(R_{\text{mid}})}{\eta_t} \frac{u_{\text{tip}}^2}{2} \frac{s_{\text{tip}}}{u_{\text{tip}}} \frac{1}{c^2} \frac{\text{LDR}(R_{\text{mid}})}{C_L^2(R_{\text{mid}})} \frac{4St^*}{K^*} = \frac{\Psi_t(R_{\text{mid}})}{\eta_t(R_{\text{mid}})} \frac{u_{\text{tip}} s_{\text{tip}}}{c^2} \frac{\text{LDR}(R_{\text{mid}})}{C_L^2(R_{\text{mid}})} \frac{2 St^*}{K^*} \quad (28)$$

As it is outlined previously, the mechanically unfavorable design case is considered when the spanwise constant PVS frequency coincides with the first bending eigenfrequency of the fan blade, posing an increased risk of blade resonance:

$$f_{\text{PVS}} = \text{const} = f_{\text{B},1} \quad (29)$$

If Equations (28) and (13) are substituted in the right-hand side and the left-hand side of Equation (29), respectively, the following equation is obtained:

$$\frac{\Psi_t(R_{\text{mid}})}{\eta_t(R_{\text{mid}})} \frac{u_{\text{tip}} s_{\text{tip}}}{c^2} \frac{\text{LDR}(R_{\text{mid}})}{C_L^2(R_{\text{mid}})} \frac{2 St^*}{K^*} = \frac{0.56}{l^2} K_b t a_b \quad (30)$$

After rearrangement, Equation (30) can be written in the following as dimensionless, from:

$$\frac{u_{\text{tip}}}{a_b} = \frac{\eta_t(R_{\text{mid}})}{\Psi_t(R_{\text{mid}})} \frac{t}{c} \left(\frac{c}{s}\right)_{\text{tip}} \frac{1}{AR^2} \frac{C_L^2(R_{\text{mid}})}{\text{LDR}(R_{\text{mid}})} K_b \frac{0.56 K^*}{2St^*} \quad (31)$$

Equation (31) provides a means for calculating the critical u_{tip}/a_b velocity ratio for which PVS results in blade resonance, if the nondimensional characteristics—valid for an entire PVS-affected rotor family under survey—are substituted into the right-hand side of the equation. With knowledge of the blade material, a_b can be obtained (cf. Equation (10) and the paragraph below), and thus, the critical u_{tip} value can be computed. Hence, critical rotor diameter \times rotor speed data couples can be discovered for an entire rotor family, consisting of rotors of various diameters and speeds.

If the rotor diameter and the nominal rotor speed are fixed for further defining a specific case study, the resultant, nominal u_{tip} value can be compared to the aforementioned critical one. Thus, it can be judged whether a risk of blade resonance may occur by changing the rotor speed, e.g., via a frequency converter. Furthermore, if the rotor diameter and the rotor speed are fixed, all dimensional quantities can be calculated, with the knowledge of nondimensional data in Table 3 as well as on the right-hand side of Equation (25). This makes possible the calculation of f_{PVS} , using Equation (25), for acoustics evaluation. By such means, the third-octave band incorporating PVS can be identified and critically evaluated. For this purpose, the A-weighting graph [49] is to be considered. The plateau of the A-weighting graph represents the most sensitive part of the human audition. Keeping f_{PVS} away from this plateau in blade design, by selecting the appropriate operational and geometrical characteristics, gives a potential for moderating the impact of fan noise on humans. If such design intent cannot be realized for modifying f_{PVS} , the PVS phenomenon in itself is to be suppressed, necessitating modifications in the blade layout, e.g., boundary-layer tripping. However, such modifications are to be treated with criticism, as, e.g., boundary layer tripping may undermine the performance of the fan [3]. Such undesired effects justify the present intent by the authors to accept the occurrence of PVS but “mistune” it toward uncritical frequencies by simple preliminary design means, as a first approach. Such mistuning, being beneficial from both vibration and noise points of view, is to be performed in the preliminary blade design by the negation—i.e., avoidance—of the worst-case design and operational scenarios represented by PVS-affected rotors. For this reason, setting up guidelines for the worst-case design scenarios is of practical value.

5. Calculation Example for the Designed Rotor

First, based on Equation (31) and data in Table 3, as it is specific to the PVS-affected rotor designed herein, the critical tip speeds are computed for various blade materials, which means different values of a_b in terms of the calculation process. The calculated values are summarized in Table 4.

Table 4. Critical rotor tip speeds.

		Steel	Aluminum	Polycarbonate
a_b	[m/s]	5000	5100	1350
$u_{tip,crit}$	[m/s]	1.80	1.83	0.49

The methodology presented herein provides a means for simply checking whether PVS may cause a risk at all from a blade resonance point of view. Based on Table 4, it can be concluded that in the present case study, the critical tip speed is sufficiently low to make these cases irrelevant for the blade resonance point of view of the first-order bending mode (Figure 6). Namely, only impractically low rotor diameters D and/or rotor speeds n would result in coincidence of the f_{PVS} and $f_{B,1}$ [Equation (10)] values for the presented case study. Furthermore, the lower the tip speed, the lower the fluctuating force causing vibration. However, the risk of blade vibration cannot be excluded for other design cases, characterized by modified data in Table 3 and for other—i.e., higher-order bending, as well as torsional—modes of vibration. Therefore, an important future task—as part of the ongoing research project—is to systematically explore risky cases (operational, geometrical, and material characteristics) from the resonance point of view. The methodology presented herein can be generally applied for such systematic studies.

The reader is reminded that the mechanical effect of the blade twist is neglected herein, cf. Section 2. With consideration of the blade twist, the first bending eigenfrequency would be less, thus reducing the impractically low critical tip speed even further.

As the second part of the calculation example, the rotor diameter and rotor speed are fixed as follows: $D_{tip} = 0.900$ m, $n = 1450$ 1/min. Such values are relevant in industrial ventilation. They result in $u_{tip} = 68.3$ m/s. Considering data in Table 4 as well as previously fixed further parameters, the additional quantities required to calculate the PVS frequency, according to Equation (28), are derived. The values of the computed quantities are presented in Table 5.

Table 5. PVS frequency for a five-bladed, $n = 1450$ 1/min axial flow fan.

D_{tip}	c	$C_L (R_{mid})$	$LDR (R_{mid})$	s_{tip}	f_{PVS}
0.900 m	0.120 m	1.30	43.5	0.565	4520 Hz

The calculated PVS frequency falls within the third-octave band of the middle frequency of 5 kHz. Thus, it approximates the plateau of the A-weighting graph. Therefore, the related noise may cause increased annoyance for a human observer. However, by modifying the design parameters, the axial fan can be redesigned to keep the PVS frequency away from the plateau of the A-weighting graph, based on the presented computation. The systematic exploration of the advantageous parameter modifications, while finding reasonable compromises with other design perspectives, is also a future task.

Based on Table 2, for the first bending eigenfrequency of the designed blade, the following value is calculated: $f_{B,1} = 116$ Hz. For the sake of completeness, the following mandatory engineering investigation is to be performed. On the one hand, is to be checked whether the computed eigenfrequency is sufficiently far from the nominal rotational frequency. The rotational speed $n = 1450$ 1/min, which corresponds to 24 Hz, is thus $\approx 20\%$ of the first bending eigenfrequency, which is satisfactory.

On the other hand, as mentioned in Section 3.1, elements located upstream of the rotor may lead to rotor–stator interaction, occurring at a frequency of rotational frequency n

multiplied by the number of upstream elements. Therefore, it is necessary to examine for which number of upstream elements (e.g., support strut, inlet guide vane) the computed eigenfrequency would coincide with the excitation frequency of the rotor–stator interaction. As $f_{B,1} \approx 5 \times 24 \text{ Hz} = 120 \text{ Hz}$, the critical element number is five, which should be avoided by all means. For example, upon demand, the application of three fan-supporting struts upstream of the rotor fulfills this condition.

6. Conclusions and Future Remarks

Based on the semi-empirical model in literature, the pessimistic design condition of spanwise constant PVS frequency is determined from an aerodynamic approach. To fulfill this condition, an iterative fan design method was elaborated, resulting in a design case study of a PVS-affected rotor. The frequency of PVS was computed with the knowledge of the global operational and geometrical characteristics of an axial fan. A calculation process for determining the eigenfrequency related to the first bending mode of vibration of a circular-arc-cambered plate blade was presented. By combining these two approaches, guidelines can be formulated, already in the preliminary design phase, for the following.

- (a) The critical tip speed that may cause resonance can be estimated for various blade materials, according to Equation (31).
- (b) On the basis of (a), the critical rotor speed n can be calculated for axial fans of known diameter. Thus, it can be judged whether a risk of blade resonance may occur by changing the rotor speed.
- (c) The expected PVS frequency can be determined by knowing the rotor speed of the fan. Therefore, the adverse acoustic effect of PVS can be forecasted on the basis of the A-weighting graph.

As a future objective, opposing the pessimistic design scenarios, redesign efforts are to be made for moderating/avoiding blade resonance and/or noise annoyance. Such efforts incorporate actions against the constancy of PVS frequency along the span. Systematic redesign scenarios as well as comparative experiments—also incorporating pessimistic, PVS-affected rotor cases—will be realized in the future for validating the methodology presented herein. The design aspects related to PVS are to be investigated in the future via studies on 2D—i.e., rectilinear—blade models as well as on truly 3D rotor blade geometries—unavoidable for full consideration of realistic rotor flow effects—by the concerted means of computational fluid dynamics (CFD), analytical mechanics, finite-element mechanical computations, and experimentation. Such studies will also serve as the exploration of the effects of assumptions and simplifications made in the method presented herein.

Author Contributions: G.D. and J.V. conceptualization, methodology, investigation, and writing. All authors have read and agreed to the published version of the manuscript.

Funding: This work has been supported by the Hungarian National Research, Development and Innovation (NRDI) Centre under contract No. NKFI K 129023. The research reported in this paper and carried out at BME has been supported by the NRDI Fund (TKP2021, project no. BME-NVA-02, TKP2021-EGA, and TKP2020 NC, Grant No. BME-NCS) based on the charter of bolster issued by the NRDI Office under the auspices of the Ministry for Innovation and Technology of Hungary. The contribution of Gábor DAKU has been supported by Gedeon Richter Talent Foundation (registered office: 1103 Budapest, Gyömrői út 19-21.), established by Gedeon Richter Plc., within the framework of the “Gedeon Richter PhD Scholarship”.

Institutional Review Board Statement: Not applicable.

Informed Consent Statement: Not applicable.

Data Availability Statement: Not applicable.

Acknowledgments: The authors are thankful to Tamás KALMÁR-NAGY for his assistance in the blade mechanics analysis.

Conflicts of Interest: The authors declare no conflict of interest.

Abbreviations

The following abbreviations are used in this manuscript:

Latin Letters

A	Cross-section [m ²]
a_b	Wave propagation speed = $(E/\rho_b)^{1/2}$ [m/s]
AR	Aspect ratio = l/c [-]
b	Transversal dist. between vortex rows [m]
c/s	Blade solidity [-]
D	Rotor diameter [m]
d_{TE}	Trailing edge thickness [m]
E	Young modulus [Pa]
F	Characteristic function
f	Dominant frequency [Hz]
g	Lateral displacement [m]
G	Shear modulus [Pa]
h	Maximum height of the camber line [m]
h/c	Relative camber [-]
i	Order number, e.g., 1, 2, 3 etc.
I	Second moment of area [m ⁴]
I_p	Polar moment of area [m ⁴]
I_t	Torsional constant [m ⁴]
K^*	Empirical coefficient ≈ 1.2 [-]
K_1	Preliminary design constant [-]
K_b	Blade mechanics coefficient [-]
K_t	Mechanical constant [-]
$K_{B,i}$	Bending mode constant [-]
c	Blade chord length [m]
c_x	Axial velocity component [m/s]
C_D	Drag coefficient [-]
C_L	Lift coefficient [-]
l	Blade span [m]
LDR	Lift-to-drag ratio = C_L/C_D [-]
N	Blade count [-]
n	Rotor speed [1/s]
R	Dimensionless radius = r/r_{tip} [-]
r	Radial coordinate [m]
Re_c	Reynolds number = $c U_0 / \nu_a$ [-]
s	Blade spacing = $2r\pi/N$ [m]
St	Strouhal number [-]
St^*	Universal Strouhal number [-]
t	Profile thickness [m]
t/c	Relative thickness [-]
u	Rotor circumferential velocity [m/s]
U_0	Free-stream velocity = $(w_1 + w_2)/2$ [m/s]
U	Length of midwall perimeter [m]
w	Relative velocity component [m/s]
W	Dimensionless free-stream velocity [-]
v	Absolute velocity component [m/s]
x, y, z	Cartesian coordinates [m]

Greek Letters

α	Angle of attack [°]
$\beta_i l$	Vibration constant $\approx (2i - 1)\pi/2$
γ	Stagger angle [°]
δ	Specific diameter [-]
ζ	Rotation angle [rad]
Δc_u	Increase of tangential velocity [m/s]
$\Delta p_{t,is}$	Isentropic total pressure rise [Pa]
η	Efficiency [-]
Θ	Momentum thickness of blade wake [m]
ν	Hub-to-tip ratio [-]
ν_a	Kinematic viscosity of air [m ² /s]
ν_p	Poisson's ratio [-]
ρ	Density [kg/m ³]
σ	Specific speed [-]
τ	Time [s]
φ	Local flow coefficient [-]
Φ	Global flow coefficient [-]
ψ	Local pressure rise coefficient [-]
Ψ	Global pressure rise coefficient [-]

Subscripts and Superscripts

1	Rotor inlet
2	Rotor outlet
a	Air
b	Blade
B	Bending
crit	Critical
i	Order-number i.e., 1, 2, 3
is	Isentropic
mid	Mid-span position
n	Order-number i.e., 1, 2, 3
PVS	Profile vortex shedding
t	Total
T	Torsional
TE	Trailing edge
tip	Blade tip

Abbreviations

2D	Two-dimensional
3D	Three-dimensional
B	Bending mode
CG	Center of gravity
CFD	Computational fluid dynamics
PVS	Profile vortex shedding
T	Torsional mode
TE	Trailing edge
VS	Vortex shedding
FEM	Finite element method

Appendix A

Table A1. Third-octave band.

Band No.	Lower Band Limit (Hz)	Center Frequency (Hz)	Upper Band Limit (Hz)
1	11.2	12.5	14.1
2	14.1	16	17.8
3	17.8	20	22.4
4	22.4	25	28.2
5	28.2	31.5	35.5
6	35.5	40	44.7
7	44.7	50	56.2
8	56.2	63	70.8
9	70.8	80	89.1
10	89.1	100	112
11	112	125	141
12	141	160	178
13	178	200	224
14	224	250	282
15	282	315	355
16	355	400	447
17	447	500	562
18	562	630	708
19	708	800	891
20	891	1000	1122
21	1122	1250	1413
22	1413	1600	1778
23	1778	2000	2239
24	2239	2500	2818
25	2818	3150	3548
26	3548	4000	4467
27	4467	5000	5623
28	5623	6300	7079
29	7079	8000	8913
30	8913	10,000	11,220
31	11,220	12,500	14,130
32	14,130	16,000	17,780
33	17,780	20,000	22,390

References

- Brooks, T.F.; Pope, D.S.; Marcolini, M.A. *Airfoil Self-Noise and Prediction*; NASA Ref. Publication: Washington, DC, USA, 1989; Volume 1218. Available online: <https://ntrs.nasa.gov/citations/19890016302> (accessed on 27 September 2021).
- Yakhina, G.; Roger, M.; Moreau, S.; Nguyen, L.; Golubev, V. Experimental and Analytical Investigation of the Tonal Trailing-Edge Noise Radiated by Low Reynolds Number Aerofoils. *Acoustics* **2020**, *2*, 293–329. [[CrossRef](#)]
- Lowson, M.; Fiddes, S.; Nash, E. Laminar Boundary Layer Aeroacoustic Instabilities. In Proceedings of the 32nd Aerospace Sciences Meeting and Exhibit, Reno, NV, USA, 10–13 January 1994; p. 10. [[CrossRef](#)]
- Balla, E.; Vad, J. A semi-empirical model for predicting the frequency of profile vortex shedding relevant to low-speed axial fan blade sections. In Proceedings of the 13th European Conference on Turbomachinery Fluid Dynamics & Thermodynamics (ETC13), Lausanne, Switzerland, 8–12 April 2019; p. 12. [[CrossRef](#)]
- Balla, E. Aerodynamic and Aeroacoustic Behavior of Axial Fan Blade Sections at Low Reynolds Numbers. Ph.D. Thesis, Department of Fluid Mechanics, Faculty of Mechanical Engineering, Budapest University of Technology and Economics, Budapest, Hungary, 2020. Available online: <http://hdl.handle.net/10890/13530> (accessed on 27 September 2021).
- Tam, C.K.W. Discrete tones of isolated airfoils. *J. Acoust. Soc. Am.* **1974**, *55*, 1173–1177. [[CrossRef](#)]
- Wright, S. The acoustic spectrum of axial flow machines. *J. Sound Vib.* **1976**, *45*, 165–223. [[CrossRef](#)]
- Nash, E.C.; Lowson, M.V.; McAlpine, A. Boundary-layer instability noise on aerofoils. *J. Fluid Mech.* **1999**, *382*, 27–61. [[CrossRef](#)]
- Ausoni, P.; Farhat, M.; Bouziad, Y.; Kueny, J.-L.; Avellan, F. Kármán vortex shedding in the wake of a 2D hydrofoil: Measurement and numerical simulation. In Proceedings of the IAHR International Meeting of WG on Cavitation and Dynamic Problems in Hydraulic Machinery and Systems, Barcelona, Spain, 28–30 June 2006; p. 14. Available online: <https://infoscience.epfl.ch/record/88122> (accessed on 27 September 2021).

10. Roger, M.; Moreau, S. Extensions and limitations of analytical airfoil broadband noise models. *Int. J. Aeroacoust.* **2010**, *9*, 273–305. [[CrossRef](#)]
11. Yarusevych, S.; Sullivan, P.E.; Kawall, J.G. On vortex shedding from an airfoil in low-Reynolds-number flows. *J. Fluid Mech.* **2009**, *632*, 245–271. [[CrossRef](#)]
12. Yarusevych, S.; Boutilier, M.S.H. Vortex Shedding of an Airfoil at Low Reynolds Numbers. *AIAA J.* **2011**, *49*, 2221–2227. [[CrossRef](#)]
13. Daku, G.; Vad, J. Experiment-Based Preliminary Design Guidelines for Consideration of Profile Vortex Shedding From Low-Speed Axial Fan Blades. *J. Turbomach.* **2021**, *143*, 061014. [[CrossRef](#)]
14. Lee, C.; Chung, M.; Kim, Y.-H. A Prediction Model for the Vortex Shedding Noise from the Wake of an Airfoil or Axial Flow Fan Blades. *J. Sound Vib.* **1993**, *164*, 327–336. [[CrossRef](#)]
15. Sasaki, S.; Kodama, Y.; Hayashi, H.; Hatakeyama, M. Influence of the karman vortex street on the broadband noise generated from a multiblade fan. *J. Therm. Sci.* **2005**, *14*, 198–205. [[CrossRef](#)]
16. Dou, H.; Li, Z.; Lin, P.; Wei, Y.; Chen, Y.; Cao, W.; He, H. An improved prediction model of vortex shedding noise from blades of fans. *J. Therm. Sci.* **2016**, *25*, 526–531. [[CrossRef](#)]
17. Paterson, R.W.; Vogt, P.G.; Fink, M.R.; Munch, C.L. Vortex Noise of Isolated Airfoils. *J. Aircr.* **1973**, *10*, 296–302. [[CrossRef](#)]
18. Arbey, H.; Bataille, J. Noise generated by airfoil profiles placed in a uniform laminar flow. *J. Fluid Mech.* **1983**, *134*, 33–47. [[CrossRef](#)]
19. Longhouse, R. Vortex shedding noise of low tip speed, axial flow fans. *J. Sound Vib.* **1977**, *53*, 25–46. [[CrossRef](#)]
20. Grosche, F.-R.; Stiewitt, H. Investigation of Rotor Noise Source Mechanisms with Forward Speed Simulation. *AIAA J.* **1978**, *16*, 1255–1261. [[CrossRef](#)]
21. Harris, C.M. *Dictionary of Architecture and Construction*, 4th ed.; McGraw-Hill Education: New York, NY, USA, 2006.
22. Castegnaro, S.; Masi, M.; Lazzaretto, A. Preliminary Experimental Assessment of The Performance of Tube-Axial Fans Designed With Different Vortex Criteria. In Proceedings of the European Conference on Turbomachinery Fluid Dynamics and hermodynamics, Stockholm, Sweden, 3–7 April 2017; European Turbomachinery Society: Lausanne, Switzerland, 2017; p. 13.
23. Masi, M.; Lazzaretto, A. A New Practical Approach to the Design of Industrial Axial Fans: Tube-Axial Fans with Very Low Hub-to-Tip Ratio. *J. Eng. Gas Turbines Power* **2019**, *141*, 101003. [[CrossRef](#)]
24. Carnegie, W. Vibrations of Pre-Twisted Cantilever Blading. *Proc. Inst. Mech. Eng.* **1959**, *173*, 343–374. [[CrossRef](#)]
25. Gruber, J.; Blahó, M.; Herzog, P.; Kurutz, I.; Preszler, L.; Vajna, Z.; Szentmártony, T. *Fans (Ventilátorok, in Hungarian)*, 2nd ed.; Műszaki Könyvkiadó: Budapest, Hungary, 1968.
26. Bohl, W. *Strömungsmaschinen 2; Berechnung und Konstruktion*; Kamprath-Reihe: Vogel Buchverlag, Germany, 1991.
27. Banerjee, J.; Williams, F. Coupled bending-torsional dynamic stiffness matrix for timoshenko beam elements. *Comput. Struct.* **1992**, *42*, 301–310. [[CrossRef](#)]
28. Sinha, S.K. Combined Torsional-Bending-Axial Dynamics of a Twisted Rotating Cantilever Timoshenko Beam with Contact-Impact Loads at the Free End. *J. Appl. Mech.* **2006**, *74*, 505–522. [[CrossRef](#)]
29. Sinha, S.K.; Turner, K.E. Natural frequencies of a pre-twisted blade in a centrifugal force field. *J. Sound Vib.* **2011**, *330*, 2655–2681. [[CrossRef](#)]
30. Sun, Q.; Ma, H.; Zhu, Y.; Han, Q.; Wen, B. Comparison of rubbing induced vibration responses using varying-thickness-twisted shell and solid-element blade models. *Mech. Syst. Signal Process.* **2018**, *108*, 1–20. [[CrossRef](#)]
31. Rao, S.S. *Vibration of Continuous Systems*; John Wiley & Sons: Hoboken, NJ, USA, 2007.
32. Gorman, D.J. *Free Vibration Analysis of Beams and Shafts*; John Wiley: New York, NY, USA, 1975.
33. Bishop, R.; Price, W. Coupled bending and twisting of a timoshenko beam. *J. Sound Vib.* **1977**, *50*, 469–477. [[CrossRef](#)]
34. Bercin, A.; Tanaka, M. Coupled Flexural-Torsional Vibrations of Timoshenko Beams. *J. Sound Vib.* **1997**, *207*, 47–59. [[CrossRef](#)]
35. Daly, B.B. *Woods Practical Guide to Fan Engineering*; Sixth Impression; Woods of Colchester Ltd.: Colchester, UK, 1992.
36. Roark, R.J.; Young, W.C.; Budynas, R.G. *Roark's Formulas for Stress and Strain*; McGraw-Hill: New York, NY, USA, 2002.
37. Blevins, R.D. *Formulas for Natural Frequency and Mode Shape*; Van Nostrand Reinhold Co.: New York, NY, USA, 1979.
38. Boresi, A.P.; Schmidt, R.J. *Advanced Mechanics of Materials*, 6th ed.; John Wiley & Sons: New York, NY, USA, 2003.
39. Hermann, T.M.; Mamarthupatti, D.; Locke, J.E. Postbuckling Analysis of a Wind Turbine Blade Substructure. *J. Sol. Energy Eng.* **2005**, *127*, 544–552. [[CrossRef](#)]
40. Mao, R.H.; Meguid, S.A.; Ng, T.Y. Finite Element Modeling of a Bird Striking an Engine Fan Blade. *J. Aircr.* **2007**, *44*, 583–596. [[CrossRef](#)]
41. Hsu, M.-C.; Akkerman, I.; Bazilevs, Y. Finite element simulation of wind turbine aerodynamics: Validation study using NREL Phase VI experiment. *Wind. Energy* **2013**, *17*, 461–481. [[CrossRef](#)]
42. Loya, J.; Rubio, M.L.; Fernandez-Saez, J. Natural frequencies for bending vibrations of Timoshenko cracked beams. *J. Sound Vib.* **2006**, *290*, 640–653. [[CrossRef](#)]
43. Balla, E.; Vad, J. Lift and drag force measurements on basic models of low-speed axial fan blade sections. *Proc. Inst. Mech. Eng. Part A J. Power Energy* **2018**, *233*, 165–175. [[CrossRef](#)]
44. Wallis, R.A. *Axial Flow Fans*; George Newnes Ltd.: London, UK, 1961.
45. Beer, F.P.; Johnston, E.R.; Mazurek, D.F. *Vector Mechanics for Engineers: Statics*, 11th ed.; McGraw-Hill: New York, NY, USA, 2016; pp. 485–572.
46. Carolus, T. *Ventilatoren*; B. G. Teubner Verlag: Wiesbaden, German, 2003.

47. Regulation of the European Commission (EU). No. 327/2011, of 30 March 2011, implementing Directive 2009/125/EC of the European Parliament and of the Council of the European Union with regard to ecodesign requirements for fans driven by motors with an electric input power between 125 W and 500 kW. *Off. J. Eur. Union* **2011**, *54*, 8–21.
48. Fathy, A.; Rashed, M.; Lumsdaine, E. A theoretical investigation of laminar wakes behind airfoils and the resulting noise pattern. *J. Sound Vib.* **1977**, *50*, 133–144. [[CrossRef](#)]
49. Norton, M.P.; Karczub, D.G. Fundamentals of Noise and Vibration Analysis for Engineers, 2nd Edition. *Noise Control. Eng. J.* **2007**, *55*, 275. [[CrossRef](#)]